Numerical Simulation of Flow-Induced Birefringence in Injection Molded Disk

H. S. Lee* · G. D. Shyu** · A.I. Isayev**

Abstract

This study is an attempt to understand the birefringence and stress development in an injection molded disk. A computer code was developed to simulate all three stages of the injection molding process – filling, packing and cooling by finite element method. The constitutive equation used here was compressible Leonov model. The PVT relationship was assumed to follow the Tait equation. The flow-induced birefringence was related to the calculated flow stresses through the linear stress-optical law. The predicted birefringence was in good agreement with the experimental results.

Key Words : birefringence, viscoelasticity, injection molding, polystyrene

1. Introduction

Compact optical disks have become increasingly used for information storage in recent years[1,2]. The optical quality of molded parts is affected by the occurrence of frozen-in birefringence. The birefringence in molded parts is recognized to appear from two main sources [3-7]. The first is flow-induced birefringence, which is a consequence of shear and normal stresses developing during cavity filling and leading to orientation of molecular chains. The second source of birefringence is nonequilibrium change of density and shrinkage, and the viscoeastic and photo-viscoelastic behavior of the polymer during the inhomogeneous rapid cooling through the glass transition temperature resulting in thermal birefringence. The birefringence of molded parts is a consequence of the interplay of these phenomena. In the melt state, the flow-induced birefringence is related to the flow stresses through the well-known linear stress-optical rule [8]. The problem of flow-induced stresses and orientation is modeled on the basis of the nonlinear viscoelastic constitutive equation [3, 4, 7, 9-20]. Isayev and Hieber [3] were among the first who proposed theoretical approach to relate the nonlinear viscoelasticity of polymers to the development of frozen-in molecular orientation (birefringence) in moldings.

Baaijens[21] and Flaman[22,23] used the compressible Leonov model, which is a nonlinear viscoelastic model, to simulate the injection molding cycle and the residual flow stresses for a strip mold.

Kwon et al. developed a numerical analysis system using a finite difference method and studied the distribution of birefringence in a center-gated disk after injection molding and injection/compression molding processing using the Leonov model [9-10].

In this study, we have developed a numerical simulation program using finite element method for the injection molding of a center-gated disk, considering all three stages of the injection molding process – filling, packing and cooling. The constitutive equation used here was compressible Leonov model [24]. The PVT relationship was assumed to follow the Tait equation. The flow stresses were calculated using the Leonov model. The flow-induced birefringence was related to the flow stresses through the linear stress-optical law [8]. The results of numerical simulation were compared with the corresponding experimental data [25]

2. Theory

2.1 Governing Equations

Very often the thickness of a cavity is much smaller than planar dimensions. Therefore, in a simulation of flow in a thin cavity, the velocity component in the gapwise direction is assumed to be equal to zero.

The momentum equations in the absence of inertia and body forces are:

---

* Chungju National University
** The University of Akron

$$\frac{\partial \sigma_{xx}}{\partial x} + \frac{\partial \sigma_{xz}}{\partial z} = 0 \qquad (1)$$

$$\frac{\partial \sigma_{yy}}{\partial y} + \frac{\partial \sigma_{yz}}{\partial z} = 0 \qquad (2)$$

where x and y are planar directions and z is the gapwise direction, and σ represents the total stress.

The continuity equation for a compressible two-dimensional flow is:

$$\frac{\partial \rho}{\partial t} + \frac{\partial}{\partial x}(\rho v_x) + \frac{\partial}{\partial y}(\rho v_y) = 0 \qquad (3)$$

where v_x and v_y are velocity components in the x and y directions and the density ρ is assume to follow the Tait equation:

$$\rho(P,T) = \rho_0(T)\left\{1 - C \ln\left[1 + \frac{T}{B(T)}\right]\right\}^{-1} \qquad (4)$$

where C is a constant and B is a function of temperature.

In a nonisothermal problem, the momentum and the continuity equations are coupled with the energy equation. Since the transverse dimension in a thin cavity is much smaller than the planar dimensions, the thermal conductivity in the planar dimensions is ignored compared to that in the gapwise direction. Then the energy equation is:

$$\rho C_p\left(\frac{\partial T}{\partial t} + v_x\frac{\partial T}{\partial x} + v_y\frac{\partial T}{\partial y}\right) = \frac{\partial}{\partial z}\left(\kappa\frac{\partial T}{\partial z}\right) + \Phi \qquad (5)$$

where C_p, κ and Φ are specific heat, thermal conductivity, and dissipation function, respectively. The dissipation function is given as

$$\Phi = 2\eta_0 s\, tr\underline{\underline{e}}^2 + \sum_k \frac{\eta_k}{4\theta_k^2}[\frac{I_1(I_2 - I_1)}{3} + tr\underline{\underline{C}}_k^2 - 3] \qquad (6a)$$

$$\text{where} \quad \underline{\underline{e}} = \frac{1}{2}(\nabla \underline{v} + \nabla \underline{v}^T). \qquad (6b)$$

$\underline{v}$ is the velocity vector, I_1 and I_2 are the invariants of the elastic strain tensor $\underline{\underline{C}}_k$, and η_k, θ_k and s are described in the following paragraph.

By employing the Leonov constitutive model, the stress field can be related to the velocity gradient field as follows:

$$\underline{\underline{\sigma}} = -P\underline{\underline{\delta}} + \eta_0 s(\nabla \underline{v} + \nabla \underline{v}^T) + \sum_k \frac{\eta_k}{\theta_k}\underline{\underline{C}}_k \qquad (7)$$

where P is the pressure, s is a rheological parameter lying between zero and one, and η_k and θ_k are the kth mode shear viscosity and relaxation time, respectively, and C_k is the elastic strain tensor for the kth mode of Leonov model. The parameters η_k and θ_k are temperature dependent quantities based on a WLF temperature shift factor

[5], namely $\eta_k(T) = \eta_k(T_0) \cdot a_T / a_{T0}$ and $\theta_k(T) = \theta_k(T_0) \cdot a_T / a_{T0}$

where

$$a_T = \begin{cases} a_{Tg} & T \le T_g \\ \exp\left[-\frac{C_1(T - T_{ref})}{C_2 + T - T_{ref}}\right] & T > T_g \end{cases} \qquad (8)$$

T_{ref} is the reference temperature, T_g is the glass transition temperature, and C_1 and C_2 are constants. The zero shear rate viscosity function η_0 is defined as

$$\eta_0 = \sum_k \eta_k / (1 - s)$$

For the two-dimensional analysis, the governing equations for the elastic strain tensor C_k are:

$$\frac{DC_{xx,k}}{Dt} = 2\frac{\partial v_x}{\partial z}C_{xz,k} - \frac{1}{2\theta_k}(C_{xx,k}^2 + C_{xz,k}^2 - 1) \quad (9)$$

$$\frac{DC_{yy,k}}{Dt} = 2\frac{\partial v_y}{\partial z}C_{yz,k} - \frac{1}{2\theta_k}(C_{yy,k}^2 + C_{yz,k}^2 - 1) \quad (10)$$

$$\frac{DC_{zz,k}}{Dt} = -\frac{1}{2\theta_k}(C_{xz,k}^2 + C_{yz,k}^2 + C_{zz,k}^2 - 1) \quad (11)$$

$$\frac{DC_{xz,k}}{Dt} = \frac{\partial v_x}{\partial z}C_{zz,k} - \frac{1}{2\theta_k}C_{xz,k}(C_{xx,k} + C_{zz,k}) \quad (12)$$

$$\frac{DC_{yz,k}}{Dt} = \frac{\partial v_y}{\partial z}C_{zz,k} - \frac{1}{2\theta_k}C_{yz,k}(C_{yy,k} + C_{zz,k}) \quad (13)$$

$$C_{xx,k}C_{yy,k}C_{zz,k} - C_{xz,k}^2 C_{yy,k} - C_{yz,k}^2 C_{xx,k} = 1 \quad (14)$$

where $\frac{DC_k}{Dt}$ is the substantial derivative of C_k with respect to time.

$$\frac{DC_k}{Dt} = \frac{\partial C_k}{\partial t} + v_x\frac{\partial C_k}{\partial x} + v_y\frac{\partial C_k}{\partial y} \qquad (15)$$

The first and second differences of normal stresses, (N_1 and N_2, respectively), are defined as:

$$N_1 = \sigma_{xx} - \sigma_{zz} \qquad (16)$$
$$N_2 = \sigma_{yy} - \sigma_{zz} \qquad (17)$$

2.2 Numerical Formulations

Solution of the governing equations with a set of appropriate boundary conditions provides the velocity and the pressure profiles. The boundary of a cavity during flow consists of a melt front, impermeable boundaries, and a gate. In the melt front, one may assume that the pressure is equal to zero and can use this as a reference pressure. In the impermeable boundary region, the melt is in contact with the boundary of the mold or insert, and the normal velocity components vanish. The flow rate is usually specified at the gate or at the entry. In addition,

symmetry boundary conditions at the centerline and no slip velocity at the solid wall of the cavity are assumed. Thus, the boundary conditions may be summarized as:

$$v_x = v_y = 0 \quad \text{at} \quad z = h \tag{18}$$

$$\frac{\partial v_x}{\partial z} = \frac{\partial v_y}{\partial z} = 0 \quad \text{at} \quad z = 0 \tag{19}$$

$$P = 0 \quad \text{at the melt front} \tag{20}$$

$$Q = Q_0 \quad \text{at the gate or entry} \tag{21}$$

Other boundary conditions on temperature are:

$$T = T_w \quad \text{at} \quad z = h \tag{22}$$

$$\frac{\partial T}{\partial z} = 0 \quad \text{at} \quad z = 0 \tag{23}$$

By substituting Eq.(7) into the Eq.(1) and (2), and integrating the results with respect to z and using the symmetric boundary conditions, Eq.(19), the velocity gradients in the absence of normal forces are:

$$\frac{\partial v_x}{\partial z} = \frac{\partial P}{\partial x} \frac{z}{\eta_x} \tag{24}$$

$$\frac{\partial v_y}{\partial z} = \frac{\partial P}{\partial y} \frac{z}{\eta_y} \tag{25}$$

where:

$$\eta_x = \eta_0 s + \frac{1}{\dfrac{\partial v_x}{\partial z}} \sum_k \frac{\eta_k}{\theta_k} C_{xz,k} \tag{26}$$

$$\eta_y = \eta_0 s + \frac{1}{\dfrac{\partial v_y}{\partial z}} \sum_k \frac{\eta_k}{\theta_k} C_{yz,k} \tag{27}$$

Integration of Eq. (24) and (25), using Eq. (18), leads to:

$$v_x = -\frac{\partial P}{\partial x} \int_z^h \frac{z'}{\eta_x} dz' \tag{28}$$

$$v_y = -\frac{\partial P}{\partial y} \int_z^h \frac{z'}{\eta_y} dz' \tag{29}$$

with substitution of Eq.(28) and (29) into the Eq. (3), the governing equation for pressure is:

$$G \frac{\partial P}{\partial t} + H - \frac{\partial}{\partial x}(S_x \frac{\partial P}{\partial x}) - \frac{\partial}{\partial y}(S_y \frac{\partial P}{\partial y}) = 0 \tag{30}$$

where:

$$G = \int_0^h (\frac{\partial \rho}{\partial P}) dz \tag{31}$$

$$H = \int_0^h (\frac{\partial \rho}{\partial T})(\frac{\partial T}{\partial t}) dz \tag{32}$$

$$S_x = \int_0^h (z \int_0^z \rho \, dz') \frac{dz}{\eta_x} \tag{33}$$

$$S_y = \int_0^h (z \int_0^z \rho \, dz') \frac{dz}{\eta_y} \tag{34}$$

The control-volume finite element method with triangular elements and linear shape functions is used to solve Eq.(30), with G and H taken to be constant in each control volume, S_x and S_y to be constant in each element.

2.3 Determination of the Elastic Strain Tensor and Birefringence

The elastic strain tensor C_k can be determined by numerical integration of the governing equations, Eq. (9) to (13). The initial values are determined from the fully developed steady-state solution, $\frac{DC_k}{Dt} = 0$, under isothermal conditions. In order to the cumbersome numerical calculations, the elastic strain C_k is determined in the streamwise coordinate system (r, θ, z), where r is the flow direction, θ is perpendicular to r in the counterclockwise direction, and z is in the gapwise direction. The corresponding elastic strains can be calculated in the global coordinate by the coordinate transformation [26]. The flow-induced birefringence in the rz plane can be calculated, according to the stress-optical law being

$$\Delta n = C_\sigma^{fl} \sqrt{N_1^2 + 4\tau_{rz}^2} \tag{35}$$

where C_σ^{fl} is the stress-optical coefficient at the melt state.

3. Results and Discussion

The simulation was based on the experiment of Yoon [25]. The material used is polystyrene (Styron 615APR/DOW), and the mold is a center gated disk. The diameter and thickness of the disk is 10.16 cm and 0.2 cm, respectively. The molding conditions are as follows: melt temperature is $225\,^{\circ}C$, mold temperature is $40\,^{\circ}C$, and volumetric flow rate is 23.8 cm^3 / s. The material data for PS used in the simulation are listed in [24]. Due to symmetry of the disk, only a quarter of the disk is considered in the simulation.

The pressure traces at various radial positions for the case of packing pressure of 15 MPa and packing time of 6.0 sec are shown in Fig. 1. Time 0.695 second marks the end of filling stage and the beginning of the packing stage. The simulation results indicate that at the start of the packing stage, the pressure in the whole cavity jumps up swiftly in about 0.07 second, giving almost the same results with the experimental data [25]. As a whole, the pressure traces predicted by using the compressible

viscoelastic model here agreed very well with the measured data [25].

The p redicted t ransient d evelopment o f t he f irst n ormal stress difference $\sigma_{rr} - \sigma_{zz}$ in the filling and packing stages is shown in Fig. 2 and 3, respectively. In the filling stage, the first normal stress difference increases with time. A peak appears near the surface due to the development of a frozen layer at t he s urface a nd t he r esulting d ecrease w ith t ime i n the available flowing channel. After 0.07 second in the packing stage, the normal stresses at the central part of the gap relax quickly since there is very little flow after 0.07 second and the temperature is still high. Later, when the temperature becomes low and the relaxation time enlarges (meaning that the induced stresses will not relax right away), the normal stresses near the midplane grow again although the flow becomes even smaller. It is noted that the normal stresses near the cavity wall does not change during the packing stage, since the temperature near the cavity wall is lower than the glass transition temperature so that the stresses have been frozen.

The predicted transient development of the second normal stress difference $\sigma_{\theta\theta} - \sigma_{zz}$ in the filling and packing stages is shown in Fig. 4 and 5, respectively. The shape of the distribution of $\sigma_{\theta\theta} - \sigma_{zz}$ is similar to that of the first normal stress difference $\sigma_{rr} - \sigma_{zz}$, but the value of $\sigma_{\theta\theta} - \sigma_{zz}$ are one order of magnitude smaller than those of $\sigma_{rr} - \sigma_{zz}$.

Fig. 6 represents the gapwise distributions of shear stress at various radial positions. Shear stress has an almost linear gapwise distribution with a slope depending on the proximity to the melt front. It decreases closer to the melt front.

Fig.7 shows the gapwise distribution of the first normal stress difference at various radial positions at the end of filling. The peaks continually decrease in magnitude and move toward the wall with increasing radial positions from the gate.

The predicted gapwise flow birefringence distribution at various radial positions at the end of filling stage is shown in Fig. 8. The birefringence shows a maximum around $z / h \cong 0.7 \sim 0.8$, like the first normal stress difference. It is noted that although the shear stress varies monotonically with z, the birefringence exhibits a peak away from the wall, due to the dominant effect of the first normal stress difference.

The predicted gapwise birefringence distribution at various radial positions at the end of packing stage with a packing pressure of 15 MPa are shown in Fig. 9. There are two peaks in the birefringence distribution; one near the

surface produced in the filling stage, the other near the center produced by the additional flow in the packing stage. The inner peak also decreases in magnitude as the radial position increases from the gate.

Without the packing stage, the predicted flow birefringence distributions at the end of cooling stage are given in Fig. 10. The birefringence at the core is zero due to the fast relaxation of the chain orientation right after filling. F ig. 1 1 i s t he c orresponding e xperimental r esults measured by Yoon [25]. It is seen that the simulation, in good agreement with the experimentation, shows appreciable birefringence at the wall and a peak which moves toward the wall with increasing radial positions from the gate.

The predicted gapwise birefringence distributions at the end of cooling stage with a packing pressure of 15 MPa are compared with experimental measurements in Fig. 12 and 13, respectively. The predicted birefringence is in good agreement with the experimental results such as the locations and magnitude of the inner peaks. However, some differences exist, such as the minimum value in the troughs, and the magnitude near the surface. Possible reasons may be due to inaccuracy in shift factors for viscosity and relaxation time at low temperatures.

The radial dependence of gapwise-averaged birefringence $< n_{\theta\theta} - n_{rr} >$ $(= \frac{1}{h} \int_0^h (n_{\theta\theta} - n_{rr})dz$) is shown in Fig. 14. $< n_{\theta\theta} - n_{rr} >$ is a monotone decreasing function of r adial p osition. S imilar d ata h ave been reported by Greener [27]. It is seen from the simulation results that packing makes $< n_{\theta\theta} - n_{rr} >$ increase significantly near the gate. Since there is less and slower material flow at larger radial positions in the packing stage, a smaller increase in $< n_{\theta\theta} - n_{rr} >$ at larger radial position due to packing is obtained.

4. Conclusions

A computer code which used the compressible Leonov model was developed to simulate the injection molding cycle. The simulation was verified with corresponding experimental measurements [25] of pressure traces, gapwise flow-induced birefringence in center- gated disk. The simulation showed that

1. The predicted birefringence was in good agreement with the experimental results such as the locations and magnitude of the peaks.

2. When the packing pressure of 15 MPa was applied, there were two peaks in the birefringence distribution; one near the surface produced in the filling stage, the other near the center produced by the additional flow in the packing stage. The inner peak decreased in magnitude as the radial position increased from the gate.

3. With the packing pressure, gapwise-averaged birefringence increased significantly near the gate. However, increment of the birefringence at larger radial position was small, since there was less and slower material flow at larger radial positions in the packing stage.

References

1. M. Ojima, A. Saito, T. Kako, M. Ito, Y.Tsunoda, S. Takayama, and Y. Sugita, Appl. Optics, 25, 483 (1986).
2. M. Takeshima and N. Funakoshi, J. Appl. Polym. Sci., 32, 3457 (1986).
3. A.I. Isayev, C.A. Hieber, Rheol. Acta., 19, 168 (1980).
4. A.I. Isayev, Ed., Injection and Compression Molding Fundamentals, Marcel Dekker, New York (1987).
5. A. I. Isayev, Ed., Modeling of Polymer Proscessing: Recent Development, Hanser, Munich (1991).
6. R. Wimbereger-Friedl, Prog. Polym. Sci., 20, 369 (1995).
7. A.I. Isayev, "Orientation Development in the Injection Molding of Amorphous Polymers", Polym. Eng. Sci., 23, 271-288 (1983).
8. H. Janeschitz-Kriegl, Polymer Melt Rheology and Flow Birefringence, Springer, Berlin (1983).
9. I.H. Kim, S.J. Park, S.T. Chung, and T.H. Kwon, Polym. Eng. Sci., 39, 1930 (1999).
10. Y. B. Lee, K. H. Kwon and K. Yoon, Polym. Eng. Sci., 42, 2246 (2002).
11. S.C. Chen, Y.C. Chen, and N.T. Cheng, Int. Comm. Heat Mass Transfer, 25, 907 (1998).
12. S.C. Chen, Y.C. Chen, and H.S. Peng, Journal of Applied Polymer Science, 75, 1640 (2000).
13. S.C. Chen, Y.C. Chen, and H.S. Peng, Adv. Polym. Tech., 21, 177 (2002).
14. N. Famili, AI. Isayev, in Modeing of Polymer Processing: Recent Developments, Hanser, Munich (1991).
15. S.C. Chen, N.T. Cheng, Y.C. Chen, SPE ANTEC Tech Papers, 38, 2590 (1992).
16. G.D. Shyu, A.I. Isayev, SPE ANTEC Tech Papers, 41, 2911 (1995).
17. S.C. Chen, Y.C. Chen, J Appl Polym Sci, 55, 1757 (1995).
18. Y.C. Chen, C.H Chen, and S.C. Chen, Polym Int, 40, 251 (1996).
19. J. S. Yu, A. H. Wagner and D. M. Kalyon, J. Appl. Polym. Sci., 44, 477 (1992).
20. X. Guo, A.I Isayev, Int Polym Process, 14, 387 (1999).
21. F.P.T. Baaijens, Rheol. Acta, 30, 284 (1991).
22. A.A. Flaman, Polym. Eng. Sci., 23, 193 (1993).
23. A.A. Flaman, Polym. Eng. Sci., 23, 202 (1993).
24. G.D. Shyu, Ph.D. Dissertation, The University of Akron (1993).
25. K. Yoon, The Korean J. Rheol., 7, 19 (1995).
26. M. Sobhanie, A.I Isayev, Rubber Chem. Tech., 62, 939 (1989)
27. J. Greener, R. Kesel, and B.A. Contestable, AIChE J., 35, 449 (1989)

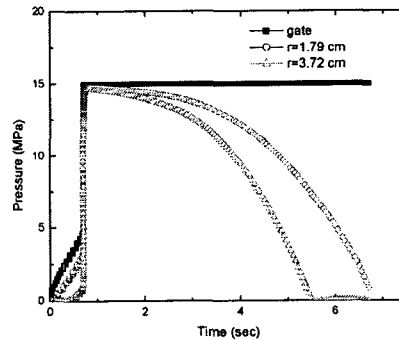Fig.1 Pressure traces at various radial positions. Molding conditions: $T_z = 225^0C$, $T_w = 40^0C$, $Q = 23.8cm^3 / s$.

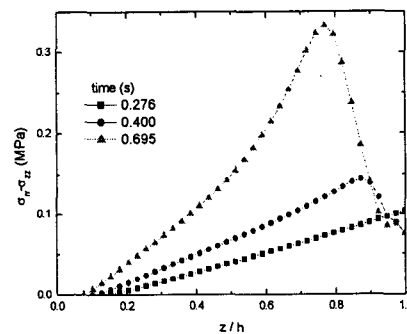

Fig.2 Predicted transient gapwise distributions of the first normal stress difference ($\sigma_{rr} - \sigma_{zz}$) at r=3.07 during filling stages.
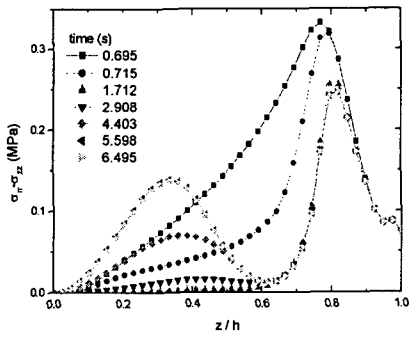
Fig.3 Predicted transient gapwise distributions of the first normal stress difference ($\sigma_{rr} - \sigma_{zz}$) at r=3.07 during packing stages.
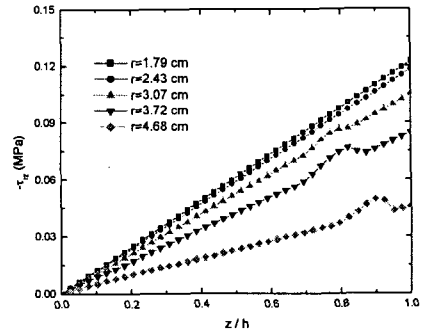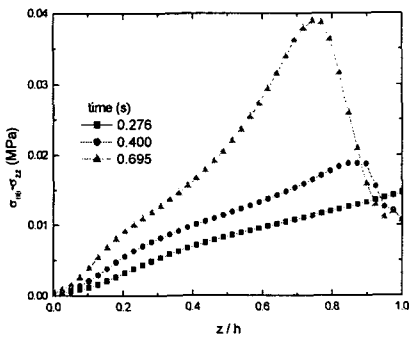

Fig.4 Predicted transient gapwise distributions of the second normal stress difference ($\sigma_{\theta\theta} - \sigma_{zz}$) at r=3.07 during filling stages.
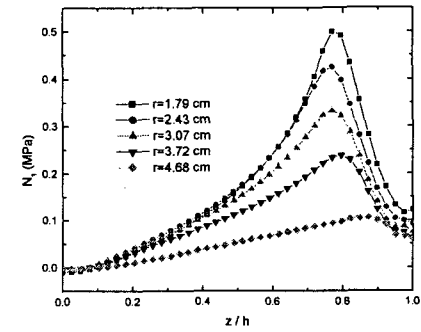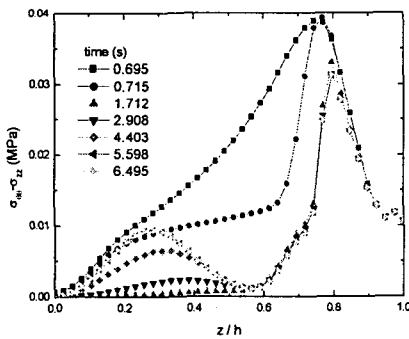

Fig.5 Predicted transient gapwise distributions of the second normal stress difference ($\sigma_{\theta\theta} - \sigma_{zz}$) at r=3.07 during packing stages.

Fig.6 Predicted gapwise distribution of shear stress τ_{rz} at various radial positions at the end of filling (t=0.694 s).

Fig.7 Predicted gapwise distribution of the first normal stress difference N_1 at various radial positions at the end of filling (t=0.694 s).
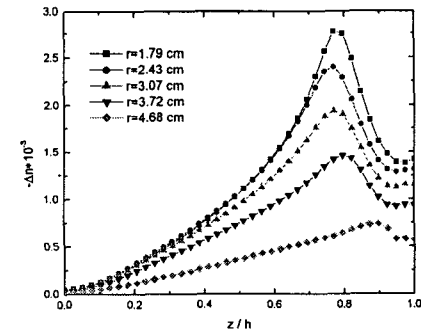
Fig.8 Predicted gapwise distribution of birefringence Δn at various radial positions at the end of filling (t=0.694 s).
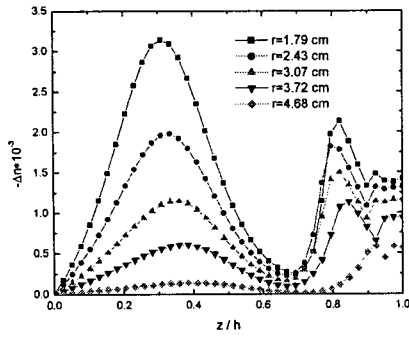
Fig.9 Predicted gapwise distribution of birefringence Δn at various radial positions at the end of packing (t=6.74 s).
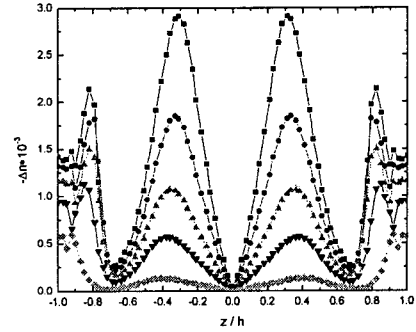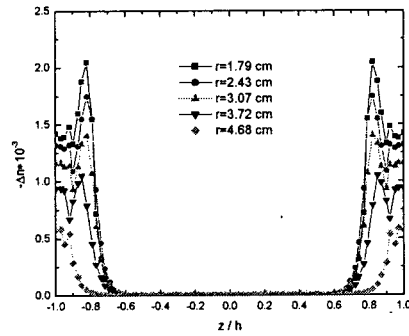

Fig.10 Predicted gapwise distribution of birefringence Δn at various radial positions at the end of cooling when no packing pressure is applied.

Fig.11 Measured gapwise distribution of birefringence Δn at various radial positions at the end of cooling when no packing pressure is applied.

Fig.12 Predicted gapwise distribution of birefringence Δn at various radial positions at the end of cooling with packing pressure of 15 MPa.
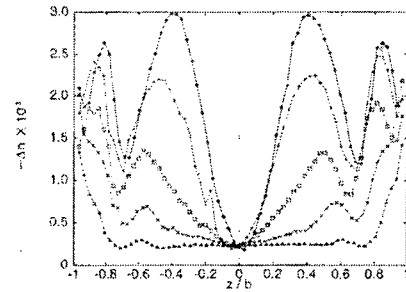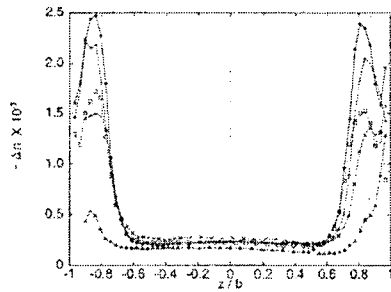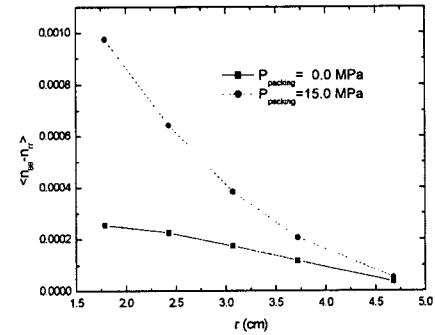

Fig.13 Measured gapwise distribution of birefringence Δn at various radial positions at the end of cooling with packing pressure of 15 MPa

Fig.14 Predicted radial profiles of gapwise-averaged residual birefringence $< n_{\theta\theta} - n_{rr} >$ with packing pressures of 0 and 15 MPa, respectively.